Supplemental Data

Supplemental Movies 1 and 2. We created movies which reproduce exactly the motion of the experimental setup and the response of the cells in Figure 1. In each movie, the raw spike signal recorded during three trials (translation, tilt and OVAR) are shown as a curve (lower blue curved) and played synchronously in the audio track. The firing rate of the neurons computed after offline spike sorting is also shown as a blue curve. A black vertical bar on the lower curves indicates the point at which the video and audio tracks are synchronous. The upper part of the movies shows an animated three-dimensional model of the experimental setup. The motion of this animated model corresponds to the actual motion of the setup which is detected by sensors mounted on the setup and recorded together with the raw spike signal. The model is a realistic representation of the actual rotator. However, the primate chair and the assembly that holds it are not represented. Instead, only a large head is drawn. The height of the whole setup is about two meters.

Each movie shows the response during 12s of tilt and translation and the first 33s of the OVAR trials shown in Figure 1. A pause of 5s is inserted between the trials. The initial position of the axes is generally different from one trial to another. In the movies, we reposition the setup accordingly in-between successive trials.

The tilt-selective cell **(Movie S1)** responds preferentially to rightward tilt and the translation-selective cell **(Movie S2)** responds to leftward acceleration. Note that, according to the equivalence principle, leftward acceleration and rightward tilt create the same activation of the otoliths. Accordingly, the translation-selective cell responds in phase with rightward tilt during steady-state OVAR. In order to make these responses visible, we added a green sphere near the right ear of the subject. During the translation trial in Movie S2, a red arrow appears when the subject undergoes leftward acceleration. The length of this arrow is proportional to the magnitude of the acceleration.

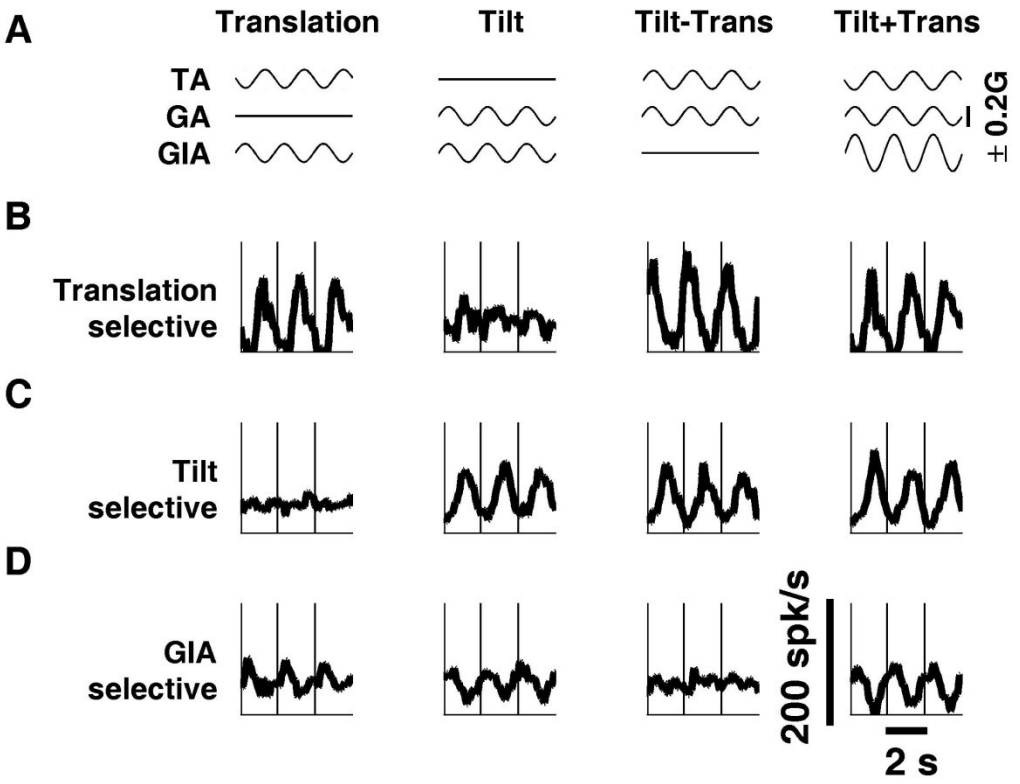

Figure S1. Tilt/translation stimuli (Angelaki et al. 1999; 2004) and example cell responses, related to Figure 1. (A) sinusoidal stimuli, which also illustrate predictions of how a cell should modulate if it selectively responded to translation ('TA' top), tilt ('GA', middle), or net gravito-inertial acceleration ('GIA', bottom). **(B)-(D)** example NU Purkinje cell responses (spike density) during translation, tilt, tilt-translation and tilt+translation. Vertical lines mark the start of each cycle. For the example cell in B, R^2_{tilt} = 0.05, R^2_{trans} = 0.85, R^2_{GIA} = 0.43. For the cell shown in C, R^2_{tilt} = 0.87, R^2_{trans} = 0.05, R^2_{GIA} = 0.49; therefore this cells was classified as tilt-selective. For the cell in D, R^2_{tilt} = 0.28, R^2_{trans} = 0.30, R^2_{GIA} = 0.82; this cell was classified as GIA-selective.

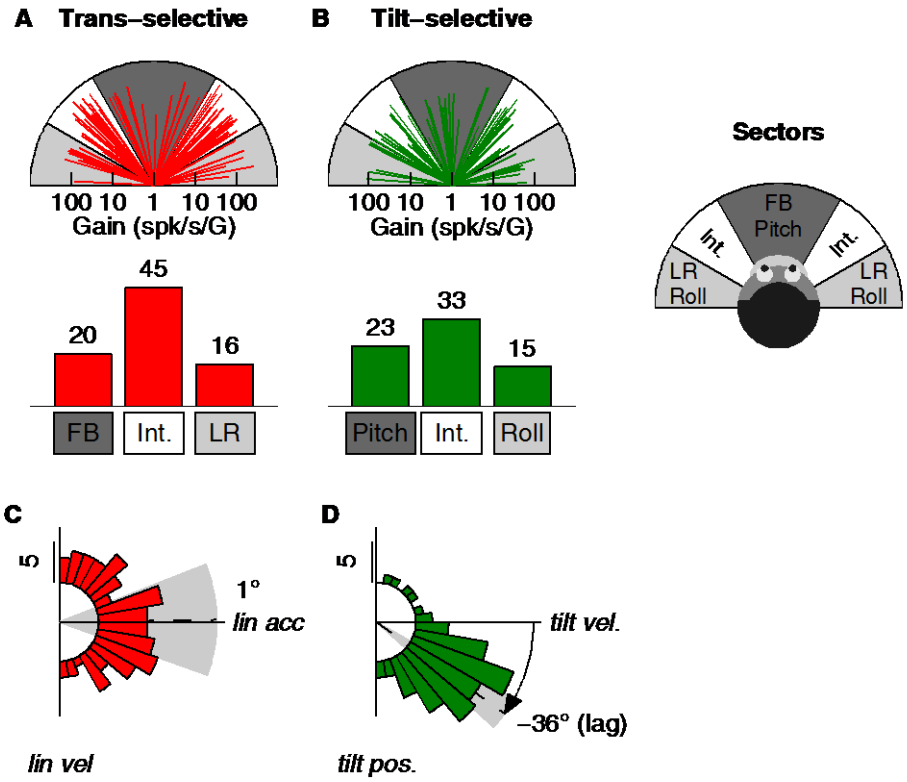

Figure S2. Distribution of preferred directions and phases, related to Figure 2. (A,B) Top: Preferred directions are shown as vectors. Bottom: The range of possible directions was divided into three sectors which cover a range of ±22.5° around the forward-backward (FB), left-right (LR) or intermediate (Int) axes (see inset 'Sectors' on right). (A) Translation preferred directions for translation-selective cells (red), (B) Tilt preferred directions for tilt-selective cells (green). Numbers indicate the number of cells observed in each sector. **(C,D)** Circular distributions of response phase. Data are shown for (C) translation response phase for translation-selective cells, and (D) tilt response phase for tilt-selective cells. Phase values are computed relative to linear acceleration (C) or tilt velocity (D). For distributions significantly different from uniform, the mean ± 95% CI (shaded area) are also shown.

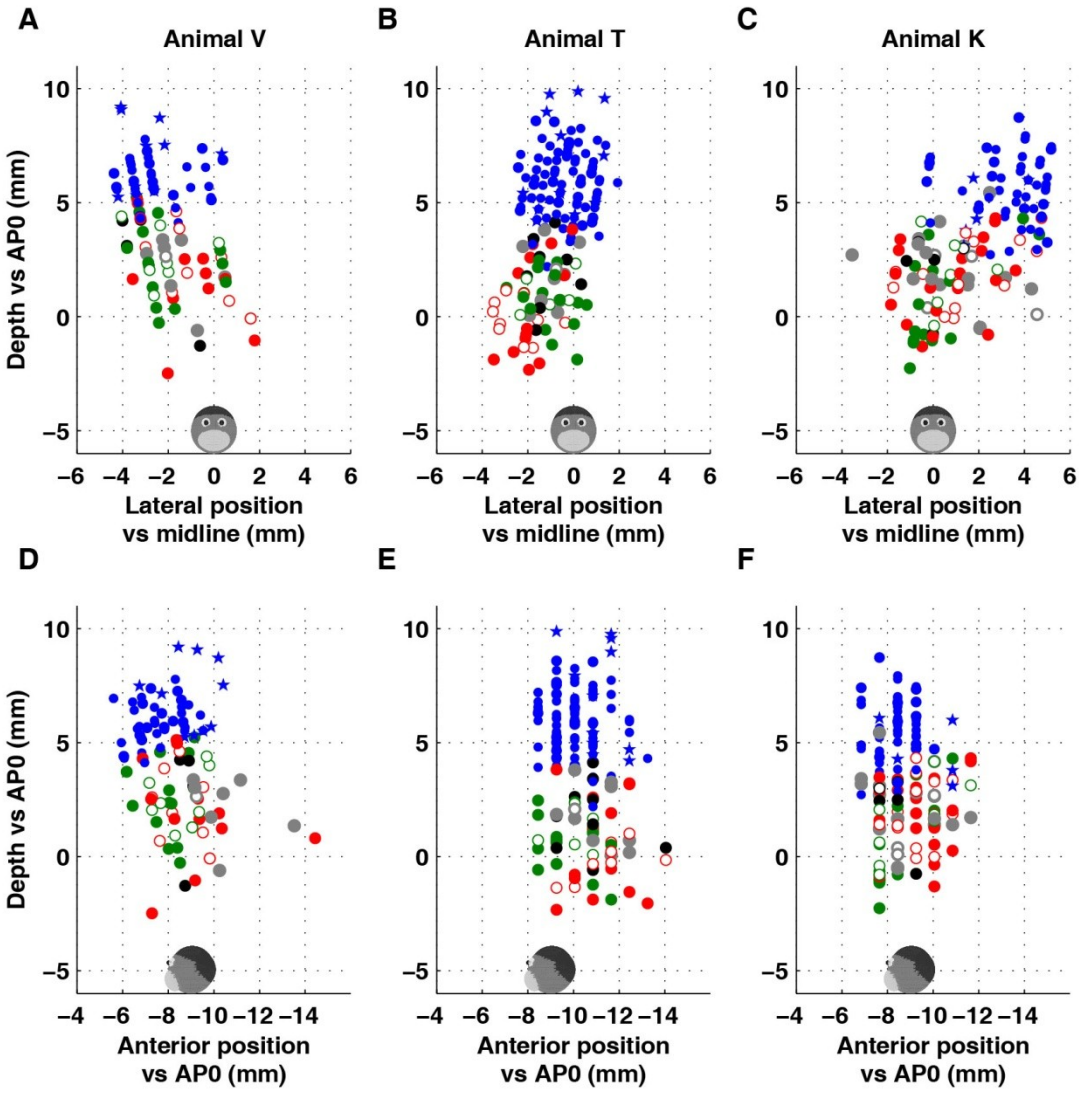

Figure S3. Reconstructed positions of the recorded cells (shown in Figure 2 and 4) in stereotaxic coordinates, related to Figure 2. (A)-(C) Frontal views; **(D)-(F)** Saggital views. Data are shown separately for each animal and each symbol corresponds to a single neuron, color-coded according to cell classification type (green: tilt-selective cells; red: translation-selective cells; black: GIA-selective cells; grey: composite cells). Open symbols represent putative Purkinje cells and filled symbols represent confirmed Purkinje cells. Eye movement-sensitive and vestibular-only cells in the cerebellar nuclei are represented as blue asterisks/circles, respectively.

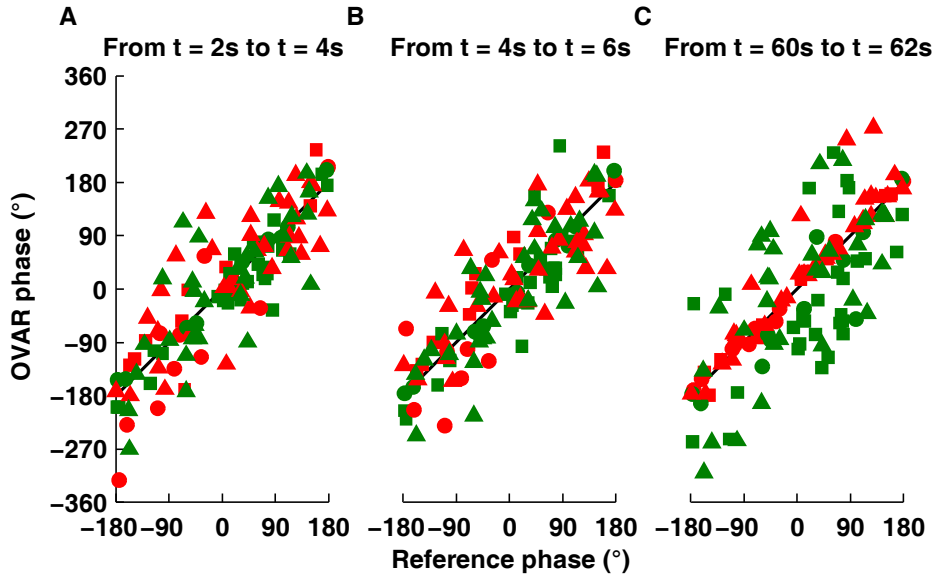

Figure S4. Comparison of the response phase during OVAR vs the 'reference' response during tilt or translation on a cell-by-cell basis, related to Figure 4. Phase of cell modulation during OVAR at **(A)** t=2-4s, **(B)** t=4-6s and **(C)** t=60-62s plotted versus the tilt (for tilt-selective Purkinje cells, n=37, green) or translation (for translation-selective cells, n=27, red) response. Two data points are shown per cell (corresponding to the two rotation directions; see Supplemental Methods). OVAR phases have been adapted by adding or subtracting 360°, such that they always fall within ±180° of the reference phase. Different symbols are used for different animals (squares: animal V; circles: animal T; triangles: animal K).

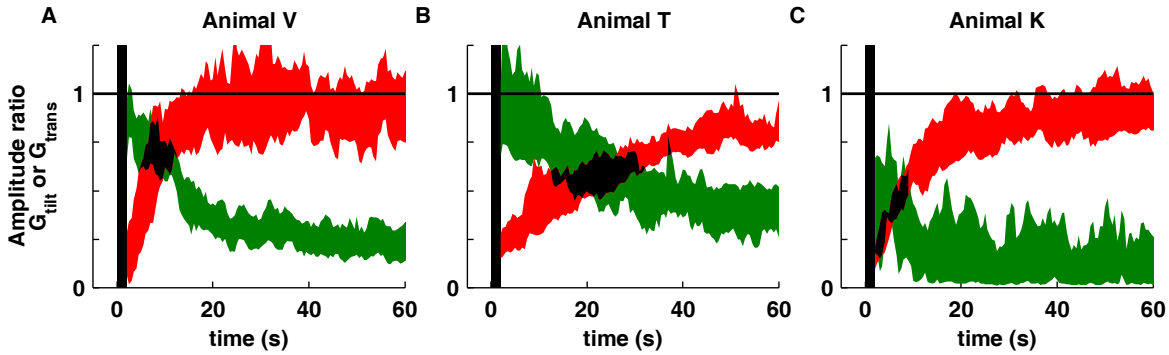

Figure S5, related to Figure 5. Time course of the gravity (GA, green) and translation (TA, red) population response in each animal (V: n= 15 tilt-selective cells and n= 5 translation-selective cells); (T: n= 6 tilt-selective cells and n= 5 translation-selective cells) (K: n= 16 tilt-selective cells and n= 17 translation-selective cells).

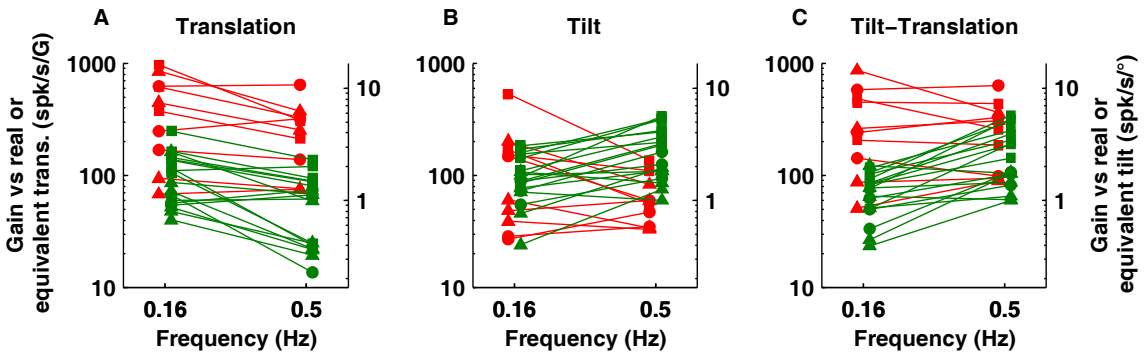

Figure S6, related to Figure 7. Frequency dependence of response gain during (A) translation, **(B)** tilt and **(C)** tilt-translation for translation-selective (red, n=10) and tilt-selective (green, n=18) Purkinje cells (squares: animal V; circles: animal T; triangles: animal K). Gain has been expressed either as spikes/s/G (left ordinate) or spikes/s/º (right ordinate). For clarity, data points for tilt-selective and translation-selective cells are plotted with a small horizontal offset.

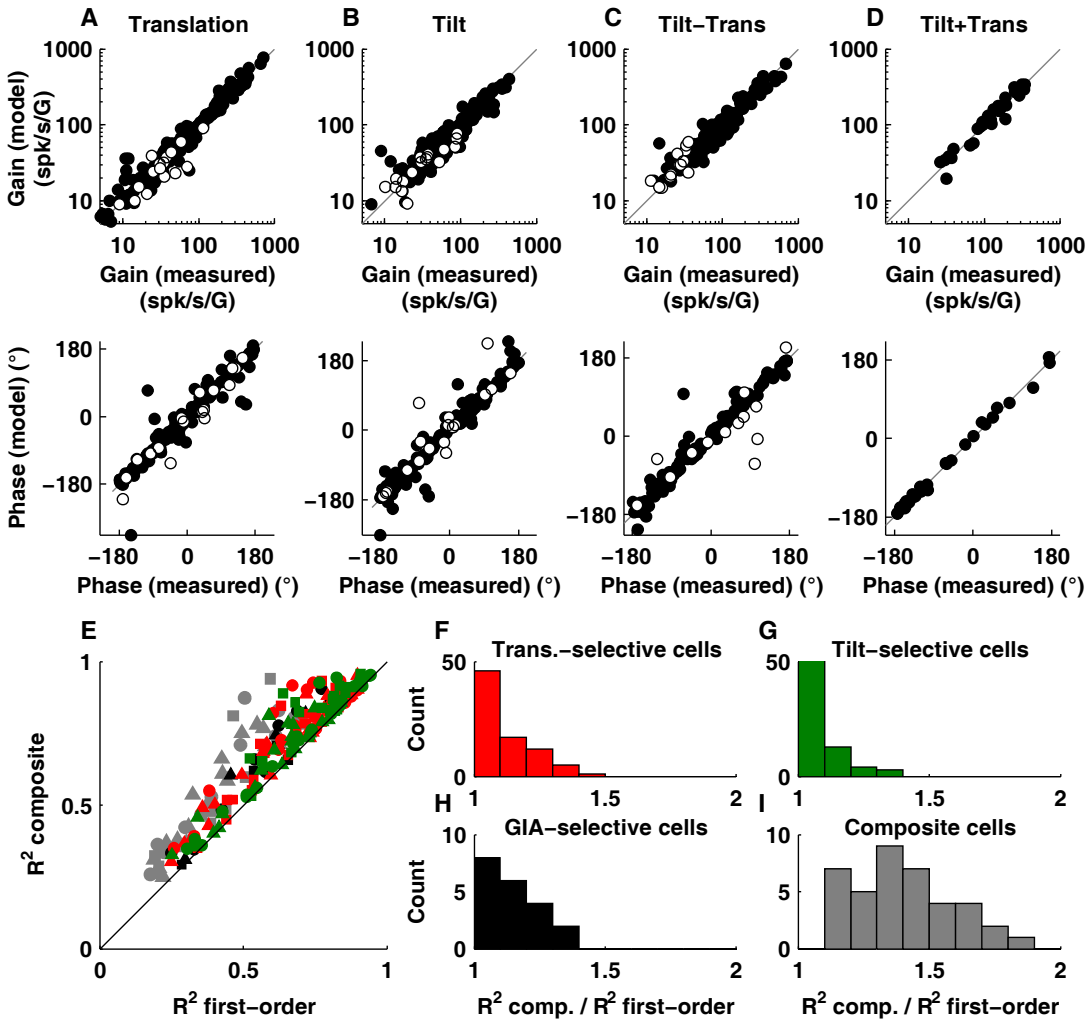

Figure S7. Accuracy of model fits, related to Figure 2. (A-D) Demonstration of the linearity assumption (necessary for the analysis shown in Figure 2). Gain (top) and phase (bottom) during **(A)** translation (n=217), **(B)** tilt (n=218), **(C)** tilt-translation (n=160) and **(D)** tilt+translation (n=31). Each cell's response is taken along the direction that is the closest to the preferred direction (thus, each cell contributes only one data point in each panel). Filled symbols: cells that passed the criterion of significant modulation, (i.e., R^2>0.25 with the composite model; see Methods). Open symbols: cells with R^2<0.25. The phase values away from the diagonal typically correspond to small gain values. **(E-I)** comparison between the goodness of fit (R^2) obtained with the composite and best first-order models. **(E)** scatter plot of both sets of R^2 values; same symbol/color code as in Figures 4 and S4. The R^2 of the composite model is always similar to or higher than the R^2 of best first-order models, as illustrated by their ratio for translation-selective **(F)**, tilt-selective **(G)**, GIA-selective **(H)** and composite **(I)** cells.

Supplemental Text

Theory and Simulations

Otolith organs in the inner ear detect the net gravito-inertial acceleration (GIA), thus cannot distinguish gravitational acceleration (GA) from translational acceleration (TA). The three semicircular canals encode rotational velocity about the three axes, yaw, pitch and roll (Figure 1B). The key assumption in models proposed to resolve the GIA ambiguity is that the brain keeps track of an internal estimate of the direction of the gravity vector relative to the head by creating ***an internal model of tilt relative to gravity*** (Mayne 1974; Borah et al 1988; Droulez & Perez 1993; Merfeld 1995; Glasauer & Merfeld 1997; Bos & Bles 2002; Zupan et al 2002; Green & Angelaki 2004; 2007; Green et al 2005; Laurens & Droulez 2007; 2008; Laurens & Angelaki 2011; Oman 1982). One way the brain can compute this 'tilt' estimate is by integrating rotational velocity information from the semicircular canals (Mayne 1974; Merfeld 1995; Angelaki et al 1999; Merfeld et al 1999; 2005; Shaikh et al 2005).

A general formula for tracking the orientation of the gravitational acceleration vector GA is through integration of rotational velocity, Ω, in three dimensions (referred to here as the **"GA estimator"**):

$$dGA(t)/dt = GA(t) \times \Omega(t)$$

or, equivalently, its integral:

$$GA(t) = \int GA(t) \times \Omega(t) dt \qquad \text{(S1)},$$

where $GA(t)$ and $\Omega(t)$ are <u>vector</u> representations of gravity and angular velocity, respectively, and 'x' denotes the vector cross-product. Equation (S1) involves three-dimensional integration, where rotations around different axes interact with one other (Green et al 2005; Green & Angelaki 2007; Laurens et al 2011). Note that a functionally-relevant tilt (gravity) signal cannot be computed by a temporal integration of canal signals alone, but instead depends on both canal and otolith cues. The intuition behind the cross-vector product in equation (S1) is that <u>only</u> the earth-horizontal (i.e., perpendicular to gravity) component of rotational velocity should contribute; i.e., *while upright*, only pitch/roll (but not yaw) rotations should update the gravity estimator. Given this GA estimate, computing TA can be done by simple subtraction (Figure 1A):

$$TA(t) = GA(t) - GIA(t) \qquad \text{(S2)},$$

Our model (Laurens & Angelaki 2011), which is based on this computation, is schematically shown in the top panel of Figure 6. The model simulates how the canals and central processing pathways produce a rotation signal $\Omega(t)$, which is integrated to produce an internal estimate of the gravity vector $GA(t)$. This estimate is used to extract

a translational acceleration signal, *TA(t),* from the net otolith input, *GIA(t)*.

Here we take advantage of a motion paradigm known as 'off-vertical axis rotation' (OVAR), to reveal the neural correlates of an internal model of gravity. This stimulus consists of rotation at constant velocity (180º/s) about a head-horizontal (yaw) axis that is tilted relative to gravity (see Figure 3 and Figure 1C). During OVAR, the head tilt relative to gravity is continuously changing (Figure 3A). In an egocentric frame of reference, the gravity vector is continuously rotating around the head (Figure 3B). This stimulus has two fundamental properties, which make it ideal for studying tilt- and translation-selective cells:

- it is a dynamic stimulus, which is equivalent to a combination of sinusoidal pitch and roll tilt (0.5 Hz). However, this tilt is accomplished through a constant-velocity yaw rotation, instead of oscillations around the pitch and roll axes. Thus, it delivers the same gravitational stimulus as pitch and roll tilt, but with a very different type of rotation.

- behavioral and theoretical studies show that, during OVAR, an initially correct tilt signal is replaced by an illusion of translation (Denise et al 1988; Guedry 1965; Wood et al 2007; Vingerhoets et al 2006; 2007). This provides an opportunity to study the interaction between cell populations, which carry internal estimates of tilt and translation signals.

The 'Canals+central processing' signal, $\Omega(t)$, in Figure 6 is computed as follows: The output of the canals, *V(t),* is initially identical to the real rotational velocity of the head, then decreases with a time constant, τ_c :

$$V(t) = [roll, pitch, yaw] = [0, 0, 180*exp(-t/\tau_c)] \quad \text{(S3)}$$

This signal is subsequently prolonged by an additional central process, known as "velocity storage" (Raphan et al 1977; Laurens & Angelaki 2011), according to:

$$dVS(t)/dt = -1/\tau_{VS}\, VS(t) + k_V\, V(t) + k_F\, GIA(t) \times GA(t) \quad \text{(S4)}$$

$$\Omega(t) = V(t)+VS(t) \quad \text{(S5)}$$

During high-velocity OVAR, the net effect of the velocity storage is to increase the time constant of rotational velocity from τ_c to τ_{VS}. Note that the term $k_F\, GIA(t) \times GA(t)$ represents a feedback loop ("velocity feedback"; Laurens & Angelaki 2011), which doesn't have any effect during high-velocity OVAR (Kushiro et al 2002; Angelaki & Hess 1996; Angelaki et al 2000; Laurens et al 2010) and isn't represented in Figure 6 (i.e., $k_F=0$; using $k_F = 0.38$ as in Laurens & Angelaki (2011) does not affect the simulation results). The other model parameters were $\tau_c = 4s$, $\tau_{VS} = 18.5s$ and $k_V = 0.22$ (Laurens & Angelaki 2011). The time constant of the velocity storage, τ_{VS}, which controls the duration of $\Omega(t)$, was determined by the evoked reflexive eye movements (horizontal

vestibulo-ocular reflex, VOR; see leftmost inset in Figure 6, bottom). Note that the actual values of these parameters contribute only to the computation of Ω(t), thus they play only a minimal role in the main properties of model simulations.

Equations (S1)-(S5) tell us that, at the beginning of constant velocity rotation, *Ω(t)* indicates the rotational velocity accurately. Thus, by integrating the earth-horizontal component of *Ω(t) (equation S1)*, the internal model can track the motion of the head relative to gravity accurately. Specifically during OVAR, the gravity estimate, *GA*, rotates together with the *GIA*. In the simulations of Figure 6, *GIA = [-sin(α)*cos(ω.t), sin(α)*sin(ω.t), -cos(α)]*, where α = 10° is the tilt angle of the axis of rotation relative to gravity and ω = 180°/s is the OVAR velocity.

However, the semicircular canals do not provide a reliable estimate of rotation speed during steady-state. Any error in the rotation velocity, *Ω(t)*, would cause an error in the tilt estimate (see (S1), (S2)). The brain corrects such errors by a feedback loop, which slowly but continuously aligns the *GA* estimate with the *GIA* (called “somatogravic feedback” in Figure 6; Laurens & Droulez 2007; Laurens & Angelaki 2011). The rationale behind this process is that long duration accelerations are very infrequent in everyday life. Therefore, averaging the *GIA* over several seconds provides a ‘default’ for gravity at low frequencies. Equivalently, the somatogravic feedback has also been modeled as a Bayesian prior centered on zero translational acceleration (Laurens & Droulez, 2007; Laurens & Angelaki 2011). This prior reflects the experience that it is more likely that we are stationary than accelerating in the world and is important for spatial orientation when robust and reliable sensory information about *Ω(t)* is missing. However, this benefit of improving the *GA* estimate during natural head movements comes at the expense of a well-known aviation illusion, where translational acceleration can be misinterpreted as tilt during prolonged (low-frequency) translation (known as the ‘somatogravic illusion’; Graybiel & Clark 1965; Curthoys 1996; Seidman & Paige 1996; Merfeld et al 2001; Clément et al 2002; Merfeld et al 2005).

The somatogravic effect can be incorporated into the model of Figure 6 by adding the low-pass filter term $1/\tau_s$ *(GIA-GA)* to the tilt estimate (a more complete presentation of this model can be found in Laurens & Angelaki (2011)). The resulting equation is:

$$dGA(t)/dt = GA(t) \times \Omega(t) - (GA(t)-GIA(t))/\tau_s \qquad \text{(S6)}$$

The time constant, τ_s, controls the gain and phase of the *GA* estimate when the otolith organs alone are activated, for example during translation-only motion and steady-state OVAR (Figure 1L,O). The dynamics of the somatogravic effect have been modeled with a time constant of 1-3 s (Bos & Bles 2002; Laurens & Angelaki 2011). Here we have used τ_s = *0.9s* for all simulations.

If the otolith organs alone are stimulated (i.e., without simultaneous canal activation, e.g., during steady-state OVAR and translation-only motion), then, according to the model of Figure 6, the somatogravic effect alone will drive the GA estimate. Specifically during low frequency translation, the GIA oscillates slowly and therefore the tilt estimate has time to fully develop (Figure 7A,B, upper panel). In contrast, at high frequencies, the somatogravic effect never fully develops as the GIA swings rapidly from one direction to the other (Figure 7B, lower panel). Thus, as expected from a low-pass filter, the tilt estimate is predicted to (1) be larger in magnitude at lower frequencies and (2) to lag the GIA increasingly more at higher frequencies. Both of these predictions are confirmed (Figure 7C,D).

Note that the somatogravic feedback is present in most models of vestibular information processing (Glasauer 1992; Merfeld 1995; Bos & Bles 2002; Zupan et al 2002) and has been predicted by optimal estimation principles (Laurens & Droulez 2007; 2008). The effects of this feedback have been observed in behavioral studies characterizing both perception (Graybiel & Clark 1965; Curthoys 1996; Seidman & Paige 1996; Merfeld et al 2001; Clément et al 2002; Merfeld et al 2005) and eye movements (Angelaki 1998; Paige & Tomko 1991).

References

Angelaki, D.E., and Hess, B.J. (1996) Three-dimensional organization of otolith- and semicircular canal-ocular reflexes in rhesus monkeys. J Neurophysiol. 75, 2425-2440.

Angelaki, D.E. (1998) Three-dimensional organization of otolith-ocular reflexes in rhesus monkeys. III. Responses To translation. J Neurophysiol. 80, 680-695.

Angelaki, D.E., McHenry, M.Q., Dickman, J.D., Newlands, S.D., and Hess, B.J. (1999). Computation of inertial motion: neural strategies to resolve ambiguous otolith information. J Neurosci 19, 316-327.

Angelaki, D.E., Merfeld, D.M., Hess, B.J. (2000) Low-frequency otolith and semicircular canal interactions after canal inactivation. Exp Brain Res. 132, 539-549.

Angelaki, D.E., Shaikh, A.G., Green, A.M., and Dickman, J.D. (2004). Neurons compute internal models of the physical laws of motion. Nature 430, 560-564.

Borah, J., Young, L.R., and Curry, R.E. (1988) Optimal Estimator Model for Human Spatial Orientation. Ann N Y Acad Sci 545, 51-73.

Bos, J.E., and Bles, W. (2002) Theoretical considerations on canal-otolith interaction and an observer model. Biol Cybern 86, 191-207.

Clément, G., Maciel, F., and Deguine, O. (2002) Perception of tilt and ocular torsion of normal human subjects during eccentric rotation. Otol Neurotol. 2002 23, 958-966.

Curthoys, I.S. (1996) The delay of the oculogravic illusion. Brain Res Bull. 40:407-410.

Denise, P., Darlot, C., Droulez, J., Cohen, B., and Berthoz, A. (1988) Motion perceptions induced by off-vertical axis rotation (OVAR) at small angles of tilt. Exp Brain Res. 73, 106-114.

Droulez, J., and Perez, V.C. (1993) Application of the Coherence Scheme to the Multisensory Fusion Problem. In: Berthoz A (ed) Multisensory Control of Movement. Oxford University Press, Oxford, pp. 485-501.

Glasauer, S. (1992) Human spatial orientation during centrifuge experiments: non-linear interaction of semicircular canals and otoliths. In: Proc XVIIth Barany Society Meeting, Jerabek, J. and Krejcova, H. eds, pp 48-52.

Glasauer, S., and Merfeld, D.M. (1997) Modelling three-dimensional vestibular responses during complex motion stimulation. In: Three-dimensional kinematics of eye, head and limb movements, Fetter, M., Haslwanter, T. and Misslisch, H., eds, (Harwood academic, Amsterdam) pp. 387-398.

Graybiel, A., Clark, B. (1965) Validity of the oculogravic illusion as a specific indicator of otolith function. Aerospace Med. 36, 1173-1181.

Green, A.M., and Angelaki, D.E. (2004). An integrative neural network for detecting inertial motion and head orientation. J Neurophysiol 92, 905-925.

Green, A.M., Shaikh AG., and Angelaki, D.E. (2005). Sensory vestibular contributions to constructing internal models of self-motion. J Neural Eng 2, S164-S179.

Green, A.M., and Angelaki, D.E. (2007). Coordinate transformations and sensory integration in the detection of spatial orientation and self-motion: from models to experiments. Prog Brain Res 165, 155-180.

Guedry, F. E. (1965). Orientation of the rotation-axis relative to gravity: its influence on nystagmus and the sensation of rotation. *Acta oto-laryngologica*,*60*(1-6), 30-48.

Kushiro, K., Dai, M., Kunin, M., Yakushin, S.B., Cohen, B., and Raphan, T. (2002) Compensatory and orienting eye movements induced by off-vertical axis rotation (OVAR) in monkeys. J Neurophysiol. 88, 2445-2262.

Laurens J., and Droulez, J. (2007). Bayesian processing of vestibular information. Biol Cybern 96, 389-404.

Laurens, J., and Droulez, J. (2008) Bayesian modeling of visuo-vestibular interactions. In: Probabilistic Reasoning and Decision Making in Sensory-Motor Systems, , Bessière, Laugier, Siegwart eds (New York: Springer) pp291–313.

Laurens, J., Straumann, D., and Hess, B.J. (2010) Processing of angular motion and gravity information through an internal model. J Neurophysiol. 104, 1370-1381.

Laurens J., and Angelaki, D.E. (2011) The functional significance of velocity storage and its dependence on gravity. Exp Brain Res 210, 407-422.

Laurens J., Strauman, D., and Hess, B.J. (2011) Spinning versus wobbling: how the brain solves a geometry problem. J Neurosci. 31, 8093-101.

Mayne, R. (1974) A systems concept of the vestibular organs. In: Handbook of sensory physiology IV/2: the vestibular system, Kornhuber HH, ed, (Berlin: Springer) pp 493-580.

Merfeld, D.M. (1995). Modeling the vestibulo-ocular reflex of the squirrel monkey during eccentric rotation and roll tilt. Exp Brain Res 106, 123-134.

Merfeld, D.M., Zupan, L.H., and Peterka. R.J. (1999). Humans use internal models to estimate gravity and linear acceleration. Nature 398, 615-618.

Merfeld, D.M., Zupan, L.H., and Gifford, C.A. (2001) Neural processing of gravito-inertial cues in humans. II. Influence of the semicircular canals during eccentric rotation. J Neurophysiol. 85, 1648-1660.

Merfeld, D.M., Park, S., Gianna-Poulin, C., Black, F.O., and Wood, S.J. (2005) Vestibular perception and action employ qualitatively different mechanisms. I. Frequency response of VOR and perceptual responses during Translation and Tilt. J Neurophysiol 94, 186-198.

Oman, C.M. (1982). A heuristic mathematical model for the dynamics of sensory conflict and motion sickness. Acta oto-laryngol supp 392, 1-44.

Paige, G.D., and Tomko, D.L. (1991) Eye movement responses to linear head motion in the squirrel monkey. I. Basic characteristics. J Neurophysiol. 65, 1170-1182.

Raphan, T., Cohen, B., and Matsuo, V. (1977) A velocity storage mechanism responsible for optokinetic nystagmus (OKN), optokinetic after-nystagmus (OKAN) and vestibular nystagmus. In: Control of gaze by brain stem neurons, Baker, R. and Berthoz, A. eds (Elsevier, Amsterdam) pp 37–47

Seidman SH, Paige GD (1996) Perception and eye movement during low-frequency centripetal acceleration. Ann N Y Acad Sci. 781, 693-695.

Shaikh AG, Green AM, Ghasia FF, Newlands SD, Dickman JD., and Angelaki, D.E. (2005) Sensory convergence solves a motion ambiguity problem. Curr Biol 15, 1657-1662.

Vingerhoets, R.A., Medendorp, W.P., and Van Gisbergen, J.A. (2006) Time course and magnitude of illusory translation perception during off-vertical axis rotation. J Neurophysiol. 95, 1571-1587.

Vingerhoets, R.A., Van Gisbergen, J.A., and Medendorp, W.P. (2007) Verticality perception during off-vertical axis rotation. J Neurophysiol. 97:3256-3268

Wood, S.J., Reschke, M.F., Sarmiento, L.A., and Clément, G. (2007) Tilt and translation motion perception during off-vertical axis rotation. Exp Brain Res. 182, 365-377

Zupan, L.H., Merfeld, D.M., and Darlot, C. (2002) Using sensory weighting to model the influence of canal, otolith and visual cues on spatial orientation and eye movements. Biol Cybern 86, 209-230.